Journal of Biomechanics 43 (2010) 1196–1201

Contents lists available at ScienceDirect

Journal of Biomechanics

journal homepage: www.elsevier.com/locate/jbiomech
www.JBiomech.com

Atomistic simulation of nanomechanical properties of Alzheimer's Aβ(1–40) amyloid fibrils under compressive and tensile loading

Raffaella Paparcone [a], Sinan Keten [a], Markus J. Buehler [a,b,*]

[a] Laboratory for Atomistic and Molecular Mechanics, Department of Civil and Environmental Engineering, Massachusetts Institute of Technology, 77 Massachusetts Ave. Room 1-235A&B, Cambridge, MA, USA
[b] Center for Computational Engineering, Massachusetts Institute of Technology, 77 Massachusetts Ave., Cambridge, MA 02139, USA

ARTICLE INFO

Article history:
Accepted 22 November 2009

Keywords:
Amyloid
Fibril
Mechanical properties
Deformation
Tension
Compression
Elasticity
Modulus
Twist angle
Molecular simulation
Nanomechanics

ABSTRACT

In addition to being associated with severe degenerative diseases, amyloids show exceptional mechanical properties including great strength, sturdiness and elasticity. However, thus far physical models that explain these properties remain elusive, and our understanding of molecular deformation and failure mechanisms of individual amyloid fibrils is limited. Here we report a series of molecular dynamics simulations, carried out to analyze the mechanical response of two-fold symmetric Aβ(1–40) amyloid fibrils, twisted protein nanofilaments consisting of a H-bonded layered structure. We find a correlation of the mechanical behavior with chemical and nanostructural rearrangements of the fibril during compressive and tensile deformation, showing that the density of H-bonds varies linearly with the measured strain. Further, we find that both compressive and tensile deformation is coupled with torsional deformation, which is manifested in a strong variation of the interlayer twist angle that is found to be proportional to both the applied stress and measured strain. In both compression and tension we observe an increase of the Young's modulus from 2.34 GPa (for less than 0.1% strain in compression and 0.2% strain in tension), to 12.43 GPa for compression and 18.05 GPa for tension. The moduli at larger deformation are in good agreement with experimental data, where values in the range of 10–20 GPa have been reported. Our studies confirm that amyloids feature a very high stiffness, and elucidate the importance of the chemical and structural rearrangements of the fibrils during deformation.

1. Introduction

Amyloid aggregation is crucial for the occurrence of several neurodegenerative disorders including Alzheimer's disease, Parkinson's disease, type II diabetes and transmissible spongiform encephalopathies (Chiti and Dobson, 2006). Amyloids form from a large class of peptides and proteins with disparate sequences through the conversion from their soluble functional states into highly organized fibrillar aggregates. X-ray diffraction patterns, experimental imaging and many other experiments have shown that amyloid fibrils feature an extensive β-sheet structure formed by fibrilized polypeptides, stabilized by a dense network of backbone hydrogen bonds (H-bonds) (Dobson, 2005; Jimenez et al., 2002; Nelson and Eisenberg, 2006). In the biophysics and biochemistry community, amyloids have been discussed as an example of a highly ordered and hierarchical material that combines elasticity, sturdiness, resistance, with the ability of providing self-assembling and self-healing properties (Gelain et al., 2006; Scheibel et al., 2003; Zhang, 2003; Zhang et al., 1993). These properties, combined with a relatively high stability even in adverse chemical environments (Zurdo et al., 2001) also render them good candidates as new nanobiomaterials (Hamada et al., 2004; MacPhee and Dobson, 2000; MacPhee and Woolfson, 2004). Several possible applications have been suggested in the literature, especially as nanowires and self-assembled nanostructures (Reches and Gazit, 2003), as natural adhesives (Mostaert et al., 2006) and as functional templates (Scheibel et al., 2003). The applications of these supramolecular assemblies exceed those of synthetic polymers since the building blocks may introduce biological functionality in addition to excellent structural and mechanical properties (Cherny and Gazit, 2008).

To improve our understanding of amyloids in their biological and pathological context as well as for biomedical and nanotechnology applications, a rigorous mechanical characterization of amyloid materials is crucial. Atomic force microscopy (AFM) based nanoindentation has provided quantitative measurements of local elasticity, since it allows the imaging of individual fibrils and the application of piconewton to nanonewton (pN–nN)

* Corresponding author at: Department of Civil and Environmental Engineering, Massachusetts Institute of Technology, 77 Massachusetts Ave., Cambridge, MA 02139, USA. Tel.: +1 617 452 2750; fax: +1 617 324 4014.
E-mail address: mbuehler@MIT.EDU (M.J. Buehler).

0021-9290/$ - see front matter © 2009 Elsevier Ltd. All rights reserved.
doi:10.1016/j.jbiomech.2009.11.026

forces. Recent reports provide values for their Young's moduli ranging from a few tens of MPa (Graveland-Bikker et al., 2006; Guo and Akhremitchev, 2006; Del Mercato et al., 2008) to several GPa (Knowles et al., 2007; Kol et al., 2005; Smith et al., 2006), depending on the size of the considered protein structure (Graveland-Bikker et al., 2006; Kol et al., 2005) and on the experimental approach and loading condition (Guo and Akhremitchev, 2006; Smith et al., 2006). AFM nanoindentation provides an indirect evaluation of the elastic properties that typically relies on some assumptions on the geometry of the fibrils, since it involves the calculation of the moment of inertia from the fibril geometry to estimate the elastic modulus. Further, experimental techniques have not yet provided insight into molecular level deformation mechanisms of amyloid fibrils under mechanical loading. Therefore, the direct calculation of the Young's moduli of amyloid fibrils by using a bottom-up molecular dynamics simulation approach is critical to identify their nanomechanical properties and to elucidate deformation mechanisms and structural changes under applied mechanical stress at different levels in the material's hierarchical structure.

Here we perform molecular dynamics simulations (MD) to study the mechanical properties of amyloid fibrils formed by the two-fold symmetric Aβ(1–40) peptide, which has been associated with Alzheimer's disease. We specifically focus on the correlation between the structural and chemical rearrangement of the fibrils under compressive and tensile loading. According to experimental imaging and NMR data (Petkova et al., 2002; Tycko, 2003), each molecule in the amyloid fibril contains two β-strands that form separate parallel β-sheets in a double-layered cross-β motif. Two such cross β-units comprise a protofilament, which shows a two-fold symmetry with respect to the fibril growth axis, as shown in Fig. 1.

2. Methods

2.1. Molecular simulation approach

Atomistic simulations are carried out using the CHARMM molecular dynamics program (Brooks et al., 1983). For modeling molecular interactions, the modified all-atom CHARMM19 polar force field is used in conjunction with an effective Gaussian model for the water solvent (Lazardis and Karplus, 1999). The initial structure (obtained as discussed in Section 2.2) is first minimized to relax the system to a favorable starting configuration, and then equilibrated at constant temperature (using an NVT ensemble) at 300 K. The minimization consists of 10,000 Steepest Descent (DS) steps followed by 50,000 Adopted Basis Newton–Raphson Method steps. The subsequent relaxation is performed using the Velocity-Verlet algorithm (VV2) for 4 ns (with a time step of 0.001 ps). No constraints are imposed to the system during energy minimization and relaxation. The relaxation is performed until the root mean square deviation (RMSD) of the protein structure remains constant, ensuring that convergence is achieved during the simulation.

2.2. Amyloid fibril geometry setup

In a recent paper we proposed a method to identify the structure of the three-fold symmetric amyloid microfibril formed by Aβ(1–40) peptide on the basis of the dependence of the energetic, chemical and structural properties on the length of the fibril (Paparcone and Buehler, 2009). The same method has been applied to identify the atomic coordinates of 91.873 Å long fibrils with the two-fold symmetric morphology, as reported in (Paparcone et al., 2009). We focus our mechanical analyses on the two-fold symmetry as it has been suggested to feature a greater stability than the three-fold symmetric structure. The amino acid sequence of the studied amyloid fibril is DAEFRHDSGYEVHHQKLVFFAEDVGSNK-GAIIGLMVGGVV (Petkova et al., 2002). Only the last 32 amino acid residues are considered here, since the first eight residues are disordered in the fibrils (Petkova et al., 2002). Therefore, the first glycine (G) along the sequence corresponds to residue #1 and it is the reference point for all residues referenced in our study. We build initial fibril geometries by imposing the typical interstrand distance of the β-sheet configuration (d=4.8 Å). Fig. 1A shows the top-view of a single layer of the amyloid fibril.

Fig. 1B and C display the amyloid fibril configuration after minimization and equilibration runs (side and top views, respectively). The structure retains its β-cross configuration, which is stabilized by the internal strong hydrophobic interactions (between the U-turns) and by a H-bond network between the layers. Each layer is twisted with respect to the previous one by θ_0=1.29° along the fibril axis, resulting in a macroscopic twist angle as it is commonly observed in amyloid fibrils (Chothia, 1973; Chou et al., 1983a; Maccallum et al., 1995; Periole et al., 2009; Salemme, 1983; Wang et al., 1996; Yang and Honig, 1995). The twist angle is in agreement with earlier theoretical results (Buchete et al., 2005). The occurrence of the twist angle is a common feature of the amyloid structures, and several explanations for its occurrence have been already suggested, including: backbone degrees of freedom (Chothia, 1973), the out-of-plane deformation of peptide groups (Salemme, 1983), intrastrand (Chou et al., 1983a; Maccallum et al., 1995) and tertiary interactions (Wang et al., 1996; Yang and Honig, 1995), as well as the tendency to minimize the surface area of the system (Koh and Kim, 2005). More recently, the analysis of the energetic implications of the twist angle in β-sheets structures suggested that the structure is stabilized by entropic contributions

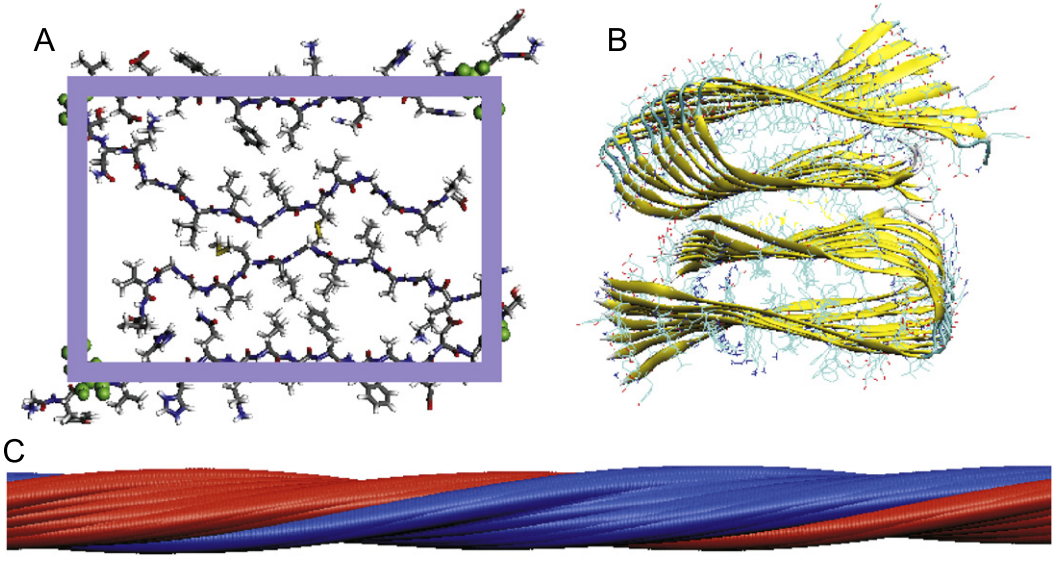

Fig. 1. Molecular and structural view of the two-fold Aβ(1–40) amyloid fibril considered in this study. Panel A: top-view of a single layer of the amyloid fibril. Each layer consists of two U-shaped protofibrils (polypeptide turns). The rectangular cross-sectional area A is approximated according to the overlapping red square, which is defined according to the positions of V4 and S18 (highlighted using the CPK green representation). Panel B shows a top-view of the amyloid fibril after equilibration, showing the characteristic twisting structure. Panel C shows a side view of the amyloid fibril, also revealing the twisted morphology. The two U-shaped polypeptide turns are colored in red and blue in this visualization to visualize the twist structure. (For interpretation of the references to the color in this figure legend, the reader is referred to the web version of this article.)

associated with an increase in backbone dynamics (Periole et al., 2009). Our observation of the emergence of the twist angle during the finite temperature equilibration phase corroborates this concept, and illustrates the importance of the backbone interactions to ensure the stability of the overall structure.

2.3. Nanomechanical characterization approach

The analysis of the nanomechanical properties is performed by carrying out MD constant force experiments to simulate the compressive and tensile deformation of the protein. In both cases, the applied load is increased in discrete steps followed by equilibration runs to simulate quasistatic loading. Fig. 2A depicts a schematic of the loading geometry, where the bottom layer of the fibril is fixed and a constant force is applied on the top in the direction of the fibril axis. Similar loading conditions have also been applied in experimental studies (Hansma et al., 2000).

The applied stress ranges between 0 and 0.13 GPa (compression) and between 0 and 0.035 GPa (tension), with variable loading steps to ensure deformation through equilibrium. The stress boundary condition is applied by imposing external forces, equally distributed among all the alpha carbon atoms composing the top layer (the total applied force is denoted by F). The applied stress σ is calculated by considering the rectangular cross-sectional area A of the fibril as represented in Fig. 1A, via $\sigma=F/A$. The cross-sectional area is defined according to the positions of the amino acids valine 4 (V4) and serine 18 (S18), highlighted in Fig. 1A using the CPK green representation. The estimated edges defining the cross-section resulted to be: h=30.56 Å and b=46.28 Å. The corresponding computed area and moment of inertia ($I=bh^3/12$) are A=1414.32 Å^2 and I=110070.81 $\times 10^{-40}$ m^4, respectively. Each simulation at a particular applied load is carried out until the system reaches stability and the RMSD converges to a constant value (within several nanoseconds). The average displacement of the bottom and top layers is used to calculate the corresponding engineering strain ε, which is evaluated when the RMSD has converged. The engineering strain ε is computed as

$$\varepsilon=\frac{d}{d_0}-1 \tag{1}$$

where d_0 and d are the top–bottom distance of the equilibrated starting structure (no load applied) and of the final compressed fibril (with load applied), respectively. The distances d_0 and d are computed by taking into account the coordinates of the center of both the top and bottom layers. Applying a continuum beam-buckling theory, the critical buckling load P_{cr} can be estimated (Hibbeler, 2005)

$$P_{cr}=\frac{\pi^2 EI}{(\alpha L)^2} \tag{2}$$

where E is the Young's modulus (such that EI is the bending stiffness), L=91.873 Å represents the effective length of the fibril and α=0.707 reflects appropriate boundary conditions. The buckling stress is calculated via $\sigma_{cr}=P_{cr}/A$.

2.4. Fibril geometry analysis under deformation

The twist angles of both the relaxed and compressed configurations are evaluated by considering the positions ($\vec{r}_{Top}$ and $\vec{r}_{Bottom}$) of the amino acid S18 of the top and bottom layers. These residues are located in the center of the U-turn of each molecule (see Fig. 1A) and are less affected by entropic perturbations during the relaxation procedure. The scalar product between the vector positions of these residues is utilized to calculate the total fibril twist angle Θ

$$\cos\Theta=\frac{\vec{r}_{Top}\cdot\vec{r}_{Bottom}}{|\vec{r}_{Top}||\vec{r}_{Bottom}|} \tag{3}$$

The interlayer twist angle is calculated by $\theta=\Theta/N$, where N denotes the number of layers in the fibril. The relative variation of the twist angle is evaluated as

$$\varepsilon_\theta=\frac{\theta}{\theta_0}-1 \tag{4}$$

where θ_0 is the initial twist angle of the relaxed structure without any load applied, and θ the twist angle at a particular load considered.

The number of H-bonds along the trajectories is computed using the software Visual Molecular Dynamics (VMD) (Humphrey et al., 1996) and imposing a cut-off distance and angle of 4.0 Å and 40°, respectively. The reported values correspond to the average number of backbone H-bonds during the last 2 ns of each simulation.

3. Results and discussion

We begin with an analysis of the stress–strain response of the amyloid fibril under compressive and tensile loading. Fig. 2B depicts the stress versus strain plot obtained from our computational experiments. In both compression and tension we observe an increase of the Young's modulus from 2.34 GPa (for less than 0.1% strain in compression and 0.2% strain in tension), to 12.43 GPa for compression and 18.05 GPa for tension. This suggests that in both compression and tension the increase in stress causes an increase of the tangent stiffness as the applied compressive or tensile strain is increased.

The obtained Young's modulus values are in close agreement with available experimental values (Knowles et al., 2007; Kol et al., 2005; Smith et al., 2006), validating the results of our simulations. Specifically for Aβ(1–42) amyloid fibrils as considered in our study, Knowles et al. reported values in the range of

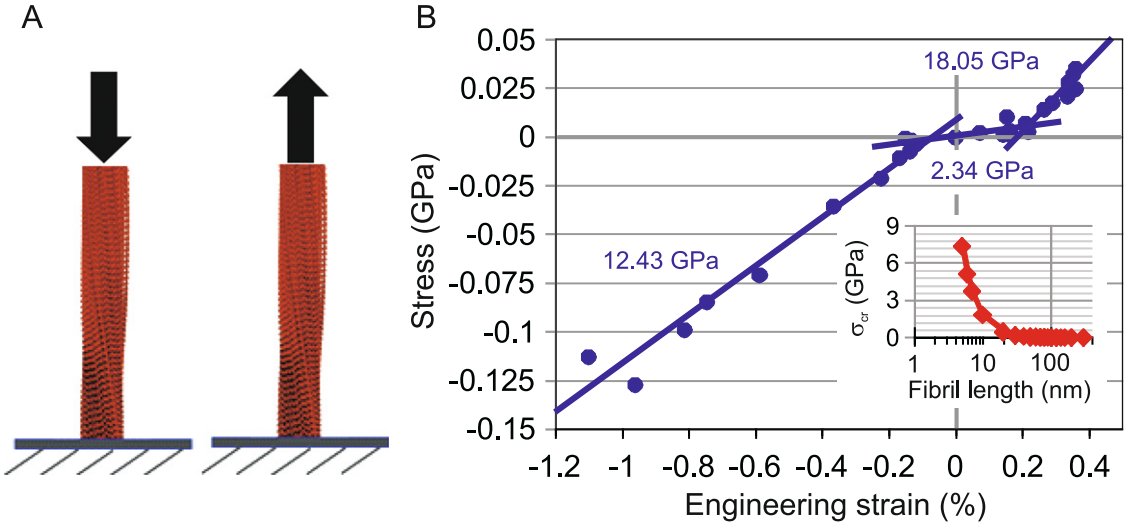

Fig. 2. Mechanical characterization of amyloid fibrils through compressive and tensile loading. Panel A: schematic representation of the compressive and tensile loading conditions. A constant stress ranging between 0 and 0.13 GPa (compression) and 0 and 0.035 GPa (tension) is applied, distributed among all C_α-atoms that form the backbone of the top protofibril layer. The C_α-atoms of the bottom layer are fixed. Panel B: stress–strain plot obtained from compression and tension simulations. The results show an increase of the stiffness in both compressive and tensile loading when the stress reaches $\approx$0.01 GPa, indicating a nonlinear stress–strain behavior. The Young's modulus ranges from 2.34 GPa (at small deformation) to 12.43 GPa under compression (for compressive strains larger than 0.1%) and 18.05 GPa under tension (for tensile strains in excess of 0.2%). These modulus values are similar as observed experimentally (Knowles, et al., 2007; Kol, et al., 2005; Smith, et al., 2006). The inlay in panel B shows the results of a buckling analysis, displaying the critical buckling stress σ_{cr} as a function of fibril length L.

12–17 GPa obtained from both experimental measurements and theoretical evaluations (Knowles et al., 2007; Kol et al., 2005; Smith et al., 2006). However, our results disagree with other experimental studies (Graveland-Bikker et al., 2006; Guo and Akhremitchev, 2006; Del Mercato et al., 2008), possibly due to different amyloid fibrils considered, or due to the experimental approach and loading conditions. Another possible reason for the decrease of the stiffness has been related to differences in the internal packing of amyloids or amyloid plaques (assemblies of fibrils), as pointed out in earlier works (Guo and Akhremitchev, 2006; Knowles et al., 2006; Nilsson and Dobson, 2003).

To elucidate the underlying molecular mechanisms of deformation, we monitor the variation of the number of backbone H-bonds as a function of the applied stress and the engineering strain, where the results are shown in Fig. 3A and B. The applied stress results in an increase of the total number of H-bonds in compression, and in a decrease of the H-bonds density when tensile loading is applied. A similar relation is found between the engineering strain and the number of H-bonds for both compression and tension.

The rearrangement of the structure is not only associated with a change of the number of backbone H-bonds as discussed in the previous paragraph, but also with a significant variation of the fibril twist angle with respect to the initial structure as shown. In Fig. 3C and D we plot the relative variation of the twist angle (as defined in Eq. (4)) as a function of the applied stress and of the engineering strain, respectively. These results clearly show that both the compressive and tensile loading are coupled with a torsional twisting deformation. The variation of the twist angle during loading is linearly proportional to both the applied stress (Fig. 3C) and the engineering strain (Fig. 3D). The corresponding fitting equations could be used to predict the deformation induced on the fibril and its resulting final periodicity as function of the applied stress or of the measured strain, in the range of small deformations. Specifically, we find that the relative variation of the twist angle ε_θ is 25.48% (per % applied strain), suggesting a remarkable change in the structural arrangement at the molecular level (see Fig. 3D).

The change in twist angle also changes the periodicity of the amyloid fibril structure as mechanical load is applied (where the periodicity is defined as $v = 360 \cdot d/\theta$ (Paparcone and Buehler, 2009), and due to the dependence of the geometric parameters on the applied strain, $v = v(\varepsilon) = 360 \cdot d(\varepsilon)/\theta(\varepsilon)$). To visualize this, in Fig. 4 we report the configurations of a ≈ 250 nm long amyloid fibril at compressive and tensile strain. The coupling of compressive and tensile deformation with torsional twisting is evident by comparing the reference structure (Fig. 4A) to the deformed fibrils (Fig. 4B and C). A similar coupling between stretching and torsional twisting has been observed in other twisted biological structures such as tropocollagen, DNA, as well as fibril and actin filaments (Bozec et al., 2007; Medved et al., 1990; Offer et al., 2002; Upmanyu et al., 2008; Weisel et al., 1987).

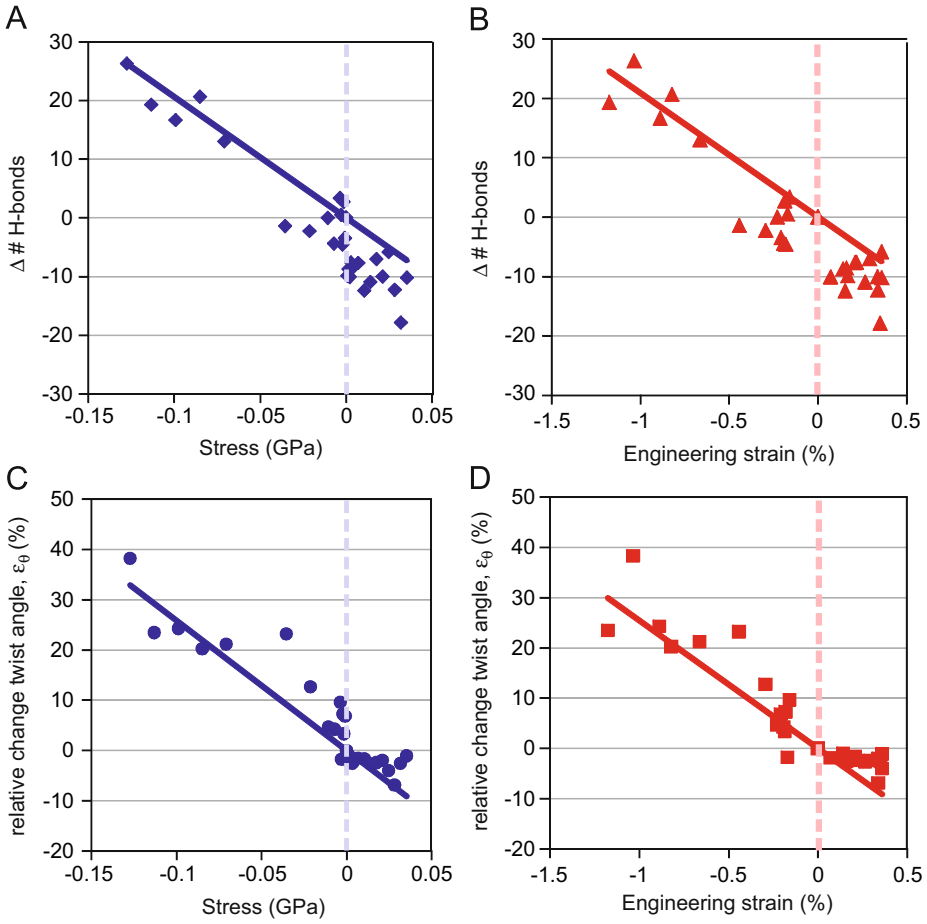

Fig. 3. Structural and chemical analysis of the amyloid fibril under compressive and tensile loading. Panels A and B: dependence of the number of backbone H-bonds on the applied stress (panel A) and on the engineering strain (panel B). Panels C and D: relative variation of the twist angle ε_θ as a function of the both the applied stress (panel C) and the engineering strain (panel D). The analysis shown in this figure suggests that compressive loading leads to an increase of the H-bond network density and to an increased twist angle, effectively reducing the periodicity of amyloid fibrils. In contrast, tensile loading has the opposite effect and leads to a decrease of both the H-bond density and twist angles, resulting in a higher overall periodicity of the fiber. Linear curves in plots are fits to the data, enforced to pass through the origin of the coordinate system.

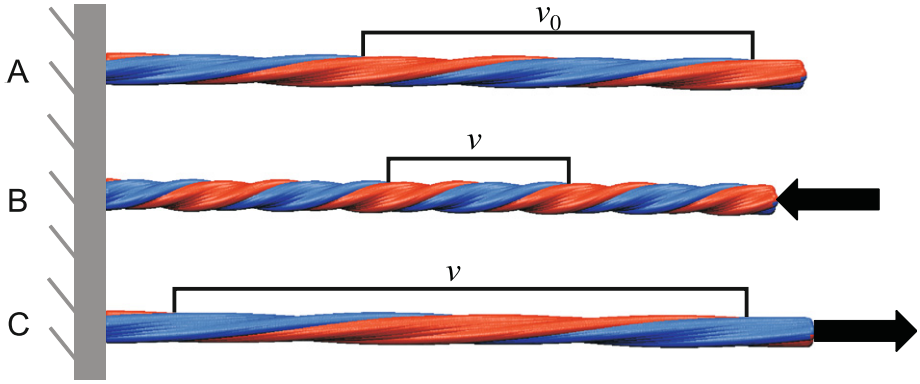

Fig. 4. Illustration of the coupling between compressive and tensile deformation and torsional twisting deformation. Panel A shows the initial configuration without load applied, while panels B and C show the deformed configuration at 4.21% compressive and 1.23% tensile strain applied. The compressive strain results in a 53.7% decrease of the periodicity v, and the tensile strain results in a 46.9% increase in v. The plots illustrate the severe change in the twist angle under compressive and tensile loads.

Since the coupling between tension and twisting has not yet been observed in experimental studies of amyloids, the predictions put forth based on our simulations provide a challenge to experimentalists to explore this aspect.

4. Conclusion

Our studies contribute to the understanding of the atomistic mechanisms that control amyloid fibril properties under compressive and tensile loading. The core finding reported in this paper is that loading in both compression and tension modes is coupled with a torsional twisting deformation, and associated with a change in the H-bond density. These molecular rearrangements of amyloid fibril result in an altered molecular configuration as the applied stress is increased. In compression, the number of H-bonds increases significantly (Fig. 3A and B), reflecting a self-strengthening mechanism that could explain why amyloid fibrils display exceptional strength properties and mechanical resilience. The significant torsional deformation under compression leads to a shear loading of the H-bond clusters, effectively resembling highly stable beta-sheet topologies (Keten and Buehler, 2008). As reported in earlier studies (Tsemekhman, et al., 2007), amyloid formation and stability strongly depends on cooperative H-bond patterns. Our results show that the response of a fibril to an external perturbation (such as compressive loading) also leads to a cooperative response of the H-bond structures. The self-strengthening feature of amyloids may be relevant to understand the mechanical compliance of amyloid fibrils in surrounding soft tissue in neurodegenerative diseases, or in the context of natural adhesives, enabling them to withstand large mechanical forces and deformation without failure. Overall, we find that the Young's moduli identified in our study are in the same order of magnitude as the experimental data (Knowles et al., 2007; Kol et al., 2005; Smith et al., 2006), in the range of 10–20 GPa. This rigidity of amyloid fibrils may be important in understanding their interactions with surrounding neuron cells, or more generally, with soft brain tissue that typically has a very low modulus of ≈ 3000 Pa, many order of magnitudes softer than that of amyloid fibrils (Miller et al., 2000).

Based on the Young's modulus obtained in compression (12.43 GPa) we predict the bending stiffness $EI = 13.2 \times 10^{-26}$ Nm^2. This result is close to results based on recent experimental values for Aβ(1–42) amyloid fibrils (Knowles et al., 2007). Based on a simple Euler buckling analysis we estimate the buckling load of the structure considered here to be $P_{cr} = 3.09 \times 10^4$ pN, which corresponds to a buckling stress of $\sigma_{cr} = 2.18$ GPa. This load is much greater than the range of stresses applied in our study (Fig. 2B), suggesting that the computational protocol to assess the compressive stiffness used here is applicable without inducing buckling, which could alter the measured modulus. The buckling loads quickly approach levels below 0.01 GPa stress for fibrils longer than 150 nm (see inlay in Fig. 2B). This suggests that for very long amyloid fibrils the stiffening regime in the stress–strain plot may not be reached under compression. More generally, buckling of long amyloid fibrils could become a governing mode of deformation that prevents the buildup of significant compressive stress levels that would lead to severe changes in the amyloid periodicity as illustrated in Fig. 3. These issues should be considered in experimental analyses.

Future studies could be focused on analyzing size-dependent properties of amyloid fibrils in both tension and compression, and could also emphasize on failure mechanisms at large loads. An interesting issue to consider will also be an analysis of the molecular mechanisms that lead to the stiffening under tension. Whereas the increase of H-bond density could explain the increase of the stiffness under compression, this concepts cannot be immediately applied to the tension case as the number of H-bonds actually decreases (Fig. 3A and B). A more detailed analysis of the strain distribution at the level of individual H-bonds could provide further insight. Other future studies could emphasize on amyloid self-assembly processes. For example, to explore a broader range of structure–property relationships of amyloid fibrils, Monte-Carlo based techniques could be applied. The confirmation of the computational predictions put forth here, specifically the coupling between axial deformation and torsional twist, represents a challenge to experimentalists that could motivate future investigations. The application of AFM techniques for both visualization and application of mechanical load may facilitate such studies and could be used to carry out an experimental analysis to confirm that loading indeed results in a significant change of the periodicity as visualized in Fig. 4.

Conflict of interest statement

None.

Acknowledgments

This research was supported by the Office of Naval Research (Grant # NN00014-08-1-0844). All authors have contributed equally to the writing of this paper.

References

Bozec, L., Heijden, G.v.d., Horton, M., 2007. Collagen fibril: nanoscale ropes. Biophys. J. 92, 70–75.

Brooks, B.R., Bruccoleri, R.E., Olafson, B.D., States, D.J., Swaminathan, S., Karplus, M., 1983. CHARMM: a program for macromolecular energy, minimization, and dynamics calculations. J. Comp. Chem. 4 (2), 187–217.

Buchete, N.V., Tycko, R., Hummer, G., 2005. Molecular dynamics simulations of Alzheimer's beta-amyloid protofilaments. J. Mol. Biol. 353, 804–821.

Cherny, I., Gazit, E., 2008. Amyloids: not only pathological agents but also ordered nanomaterials. Angew. Chem. Int. Ed. 47, 4062–4069.

Chiti, F., Dobson, C.M., 2006. Protein misfolding, functional amyloid, and human disease. Annu. Rev. Biochem. 75, 333–366.

Chothia, C., 1973. Conformation of twisted Beta-pleated sheets in proteins. J. Mol. Biol. 75, 295–302.

Chou, K.C., Nemethy, G., Scheraga, H.A., 1983a. Role of interchain interactions in stabilization of the right-handed twist of beta-sheets. J. Mol. Biol. 168, 389-407.

Del Mercato, L.L., Maruccio, G., Pompa, P.P., Bochicchio, B., Tamburro, A.M., Cingolani, R., Rinaldi, R., 2008. Amyloid-like fibril in elastin-related polypeptides: structural characterization and elastic properties. Biomacromolecules 9, 796–803.

Dobson, C.M., 2005. Structural biology prying into prions. Nature 435, 747–749.

Gelain, F., Bottai, D., Vescovi, A., Zhang, S., 2006. Designer self-assembling peptide nanofiber scaffolds for adult mouse neural stem cell 3-dimensional cultures. PLoS ONE 1 e119.

Graveland-Bikker, J.F., Schaap, I.A.T., Schmidt, C.F., Kruiff, C.G.d., 2006. Structural and mechanical study of a self-assembling protein nanotube. Nano Lett. 6 (4), 616–621.

Guo, S., Akhremitchev, B.B., 2006. Packing density and structural heterogeneity of insulin amyloid fibrils measured by AFM nanoindentation. Biomacromolecules 7, 1630–1636.

Hamada, D., Yanagihara, I., Tsumoto, K., 2004. Engineering amyloidogenicity towards the development of nanofibrillar materials. Trends Biotechnol. 22, 93–97.

Hansma, H.G., Pietrasanta, L.I., Auerbach, I.D., Sorenson, C., Golan, R., Holden, P.A., 2000. Probing biopolymers with the atomic force microscope: a review. J. Biomater. Sci. Polym. 11 (7), 675–683.

Hibbeler, R.C., 2005. In: Statics and Mechanics of Materials. Prentice Hall, Englewood Cliffs, NJ.

Humphrey, W., Dalke, A., Schulten, K., 1996. VMD—visual molecular dynamics. J. Mol. Graphics 14, 33–38.

Jimenez, J.L., Nettleton, E.J., Bouchard, M., Robinson, C.V., Dobson, C.M., Saibil, H.R., 2002. The protofilament structure of insulin amyloid fibrils. Proc. Natl. Acad. Sci. USA 99, 9196–9201.

Keten, S., Buehler, M.J., 2008. Geometric confinement governs the rupture strength of H-bond assemblies at a critical length scale. Nano Lett. 8 (2), 743–748.

Knowles, T.P., Fitzpatrick, A.W., Meehan, S., Mott, H.R., Vendruscolo, M., Dobson, C.M., Welland, M.E., 2007. Role of intermolecular forces in defining properties of protein nanofibrils. Science 318 (5858), 1900–1902.

Knowles, T.P.J., Smith, J.F., Craig, A., Dobson, C.M., Welland, M.E., 2006. Spatial persistence of angular correlations in amyloid fibrils. Phys. Rev. Lett. 96, 238301.

Koh, E., Kim, T., 2005. Minimal surface as a model of beta-sheets. Proteins 61, 559–569.

Kol, N., Adler-Abramovich, L., Barlam, D., Schneck, R.Z., Gazit, E., Rousso, I., 2005. Self-assembled peptide nanotubes are uniquely rigid bioinspired supramolecular structures. Nano Lett. 5, 1343–1346.

Lazardis, T., Karplus, M., 1999. Effective energy function for proteins in solution. Proteins: Struct., Funct. Bioinformatics 35 (2), 133–152.

Maccallum, P.H., Poet, R., Milnerwhite, E.J., 1995. Coulombic attractions between partially charged main-chain atoms stabilise the right-handed twist found in most beta-strands. J. Mol. Biol. 248, 374–384.

MacPhee, C.E., Dobson, C.M., 2000. Formation of mixed fibrils demonstrates the generic nature and potential utility of amyloid nanostructures. J. Am. Chem. Soc. 122, 12707–12713.

MacPhee, C.E., Woolfson, D.N., 2004. Engineered and designed peptide-based fibrous biomaterials. Curr. Opin. Solid State Mater. Sci. 8, 141–149.

Medved, L., Ugarova, T., Veklich, Y., Lukinova, N., Weisel, J.W., 1990. Electron microscope investigation of the early stages of fibrin assembly: twisted protofibrils and fibers. J. Mol. Biol. 216, 503–509.

Miller, K., Chinzei, L., Orssengo, G., Bednarz, P., 2000. Mechanical properties of brain tissues in vivo: experiment and computer simulation. J. Biomech. 33 (11), 1369–1376.

Mostaert, A.S., Higgins, M.J., Fukuma, T., Rindi, F., Jarvis, S.P., 2006. Nanoscale mechanical characterisation of amyloid fibrils discovered in a natural adhesive. J. Biol. Phys. 32, 393–401.

Nelson, R., Eisenberg, D., 2006. Recent atomic models of amyloid fibril structure. Curr. Opin. Struct. Biol. 16, 260–265.

Nilsson, M.R., Dobson, C.M., 2003. Chemical modification of insulin in amyloid fibrils. Protein Sci. 12 (11), 2637–2641.

Offer, G., Hicks, M.R., Woolfson, D.N., 2002. Generalized Crick equations for modeling noncanonical coiled coils. Struct. Biol. 137, 41–53.

Paparcone, R., Buehler, M.J., 2009. Microscale structural model of Alzheimer Abeta(1–40) amyloid fibril. Appl. Phys. Lett. 94, 243904.

Paparcone, R., Sanchez, J., Buehler, M.J., 2009. Comparative study of polymorphous Alzheimer's Abeta(1–40) amyloid nanofibrils and microfibers. J. Comput. Theor. Nanosci. accepted for publication (in press).

Periole, X., Rampioni, A., Vendruscolo, M., Mark, A.E., 2009. Factors that affect the degree of twist in beta-sheet structures: a molecular dynamics simulation study of a cross-beta filament of the GNNQQNY peptide. J. Phys. Chem. B 113, 1728–1737.

Petkova, A.T., Ishii, Y., Balbach, J.J., Anzutkin, O.N., Leapman, R.D., Delaglio, F., Tycko, R., 2002. A structural model for Alzheimer's beta-amyloid fibril based on experimental constraints from solid state NMR. PNAS 99 (26), 16742–16747.

Reches, M., Gazit, E., 2003. Casting metal nanowires within discrete self-assembled peptide nanotubes. Science 300, 625–627.

Salemme, F.R., 1983. Structural properties of protein beta-sheets. Prog. Biophys. Mol. Biol. 42, 95–133.

Scheibel, T., Parthasarathy, R., Sawicki, G., Lin, X.M., Jaeger, H., Lindquist, S.L., 2003. Conducting nanowires built by controlled self-assembly of amyloid fibrs and selective metal deposition. PNAS 100 (8), 4527–4532.

Smith, J.F., Knowles, T.P., Dobson, C.M., Welland, M.E., 2006. Characterization of the nanoscale properties of individual amyloid fibrils. Proc. Natl. Acad. Sci. USA 43 (103), 15806–15811.

Tsemekhman, K., Goldschmidt, L., Eisenberg, D., Baker, D., 2007. Cooperative hydrogen bonding in amyloid formation. Protein Sci. 16, 761–764.

Tycko, R., 2003. Insights into the amyloid folding problem from solid-state NMR. Biochemistry 42 (11), 3151–3159.

Upmanyu, M., Wang, H.L., Liang, H.Y., Mahajan, R., 2008. Strain-dependent twist–stretch elasticity in chiral filaments. J. R. Soc. Interface 5 (20), 303–310.

Wang, L., Oconnell, T., Tropsha, A., Hermans, J., 1996. Molecular simulations of beta-sheet twisting. J. Mol. Biol. 262, 283–293.

Weisel, J.W., Nagaswami, C., Makowski, L., 1987. Twisting of fibrin fibers limits their radial growth. Proc. Natl. Acad. Sci. USA 84, 8991–8995.

Yang, A.S., Honig, B., 1995. Free energy determinants of secondary structure formation: I. alpha-helices. J. Mol. Biol. 252, 366–376.

Zhang, S., 2003. Fabrication of novel biomaterials through molecular self-assembly. Nat. Biotechnol. 21, 1171–1178.

Zhang, S., Holmes, T., Lockshin, C., Rich, A., 1993. Spontaneous assembly of a self-complementary oligopeptide to form a stable macroscopic. Proc. Natl. Acad. Sci. USA 90, 3334.

Zurdo, J., Guijarro, J.I., Dobson, C.M., 2001. Preparation and characterization of purified amyloid fibrils. J. Am. Chem. Soc. 123, 8141–8142.